Dynamics of the MoVTeNb Oxide M1 Phase in Propane Oxidation

Almudena Celaya Sanfiz,[†] Thomas W. Hansen,[†,§] Detre Teschner,[†] Peter Schnörch,[†] Frank Girgsdies,[†] Annette Trunschke,*[,†] Robert Schlögl,[†] Ming Hong Looi,[‡] and Sharifah Bee Abd Hamid[‡]

Department of Inorganic Chemistry, Fritz Haber Institute of the Max Planck Society, Faradayweg 4-6, D-14195 Berlin, Germany, and COMBICAT, University Malaya, 50603 Kuala Lumpur, Malaysia

Received: September 29, 2009; Revised Manuscript Received: December 2, 2009

Effects of framework and near surface composition of quinternary, phase-pure M1 MoVTeNb oxide catalysts on their catalytic performance in selective oxidation of propane to acrylic acid have been studied. The catalysts were prepared by hydrothermal synthesis, spray-drying, and superheated water vapor treatment. Electron microscopy, chemical analysis, nitrogen physisorption, and in situ photoelectron spectroscopy have been used to characterize the materials. The yield of acrylic acid normalized to the specific surface area of the catalyst increases with decreasing percentage of Mo and increasing molar ratio of Te/V at the surface. The metal stoichiometry at the surface differs from the stoichiometry in the crystalline bulk and changes in response to the composition of the gas phase. In situ valence band spectroscopy at 623 K in the presence of all reactants revealed a substantial covalent character of the metal−oxygen bonds in M1. The surface restructuring under formation of V- and Te-containing clusters anchored on crystalline, semiconducting M1 is, therefore, considered to establish structurally and electronically isolated active sites. The mobility of Te especially in the presence of water vapor may contribute to the development of site isolation under reaction conditions and to the enhanced selectivity to acrylic acid in the presence of steam in the feed.

Introduction

Direct oxidation of propane is an alternative albeit challenging approach[1–3] for replacing the current industrial two-stage oxidation process, in which propylene is used as feedstock to produce acrylic acid.[4,5] Efficient catalysts for selective oxidation of propane should be able simultaneously to activate the stable C−H bonds of the saturated hydrocarbon, provide oxygen atoms for insertion, and accommodate suitable acid−base properties to control the desorption of the desired reaction product avoiding further oxidation. Among all catalysts proposed to date,[1–3] MoVTe(Sb)Nb(Ta) mixed metal oxides have been found to be the most promising, achieving yields of acrylic acid of about 50% for the Te- and Nb-containing material.[6] The multicomponent metal oxides are nanocrystalline solids consisting of mainly two orthorhombic phases, called "M1" and "M2", respectively.[7]

The refinement of MoVTeNb oxide M1 and M2 structures has been reported by De Santo et al.[8] The M1 structure is illustrated in Scheme 1 that shows a two-dimensional projection of the polyhedral network in the crystallographic (001) plane and a stick-and-ball model adopted from ref 8. Corner-linked MO_6 (M = Mo, V) octahedra are two-dimensionally assembled, forming six- and seven-membered rings. Niobium has been reported to be mainly located in the center of a MO_7 pentagonal bipyramidal configuration, sharing edges with the surrounding octahedra.[8,9] The {001} planes formed by networking the polyhedrons are congruently stacked along the crystallographic [001] direction by sharing corner oxygen atoms, thereby giving rise to a prismatic particle morphology and a channel-like structure. The {001} planes of the M1 structure are arranged perpendicular to the length axis of the crystals representing the basal planes of the prisms. The heptagonal and hexagonal channels are partially occupied by finite $(TeO)_n$ zigzag chains.[8,10] The occupancy of the channels depends on the Te content and the preparation of M1. De Santo et al. reported 80% and 20% occupancy for the hexagonal and heptagonal channels, respectively.[8] The heptagonal channels in the hydrothermally prepared M1 studied by Murayama et al. were empty.[10] The Te atoms in the hexagonal channel are bound to four oxygen atoms in distorted trigonal bipyramidal coordination, assuming that the active lone pair occupies the fifth coordinate position in the

SCHEME 1: Two-Dimensional Projection of the Polyhedral Network in the Crystallographic (001) Plane (Right) and Stick-and-Ball Model (Left) of the M1 Structure

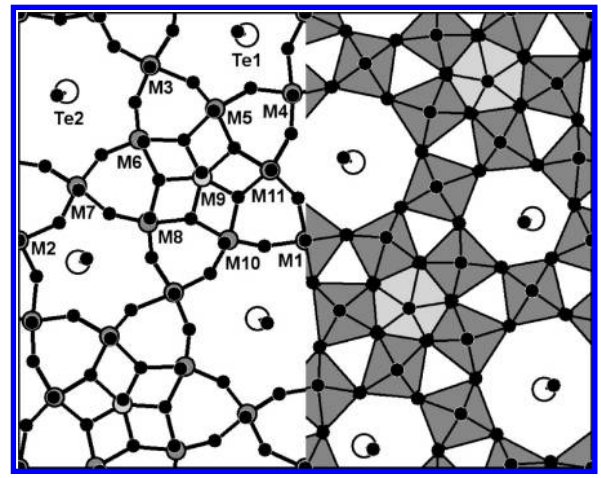

* Corresponding author. Phone: +49-30-8413-4457. Fax: +49-30-8413-4405. E-mail: trunschke@fhi-berlin.mpg.de.
[†] Fritz Haber Institute of the Max Planck Society.
[‡] University Malaya.
[§] Present address: Center for Electron Nanoscopy, Technical University of Denmark, Fysikvej Building 307, DK-2800 Kongens Lyngby, Denmark.

10.1021/jp909352u
Published on Web 01/07/2010

equatorial plane. Such a coordination and the Te−O distances ranging from 1.93 to 2.18 Å are typical for Te(IV) oxides.[11] In the heptagonal channel, $(TeO)_n$ oligomers have been refined to be arranged near the center with distances >3 Å between the Te atom in the chain and the oxygen atoms in the polyhedrons forming the channel wall.[8] The Te-rich M2 phase is less complex, being composed exclusively of corner-linked octahedra that are connected in the (001) plane, forming six-membered rings occupied by $(TeO)_n$ chains. Formulas of the refined unit cells have been reported to be $Mo_{7.8}V_{1.2}NbTe_{0.937}O_{28.9}$ for M1 and $Mo_{4.31}V_{1.36}Te_{1.81}Nb_{0.33}O_{19.81}$ for M2, respectively.[8]

M1 is known to be the most efficient phase in propane oxidation.[12–15] The role of the elements constituting the M1 phase has been studied by comparing the catalytic properties of an orthorhombic ternary MoV phase structurally similar to that of M1 with M1 composed of Mo, V, Te, and Nb.[14,16,17] The MoV oxide shows high activity but poor selectivity in propane oxidation to acrylic acid. Introduction of tellurium resulted in the development of selectivity toward acrylic acid. This effect has been attributed to the formation of tellurium-containing active sites responsible for further oxidation of propylene formed in the initial oxidative dehydrogenation of propane mediated by isolated vanadyl species. Improvements in the selectivity achieved by addition of niobium have been ascribed to spatial isolation of the alkane activating vanadium sites by breaking V−O−V bonds and achieving site isolation as an essential feature of oxidation catalysts that are selective also at high conversions.[18] The few kinetic experiments performed so far on MoVTe(Sb)Nb oxides show that the rate-determining step in propane oxidation to acrylic acid is the activation of the first C−H bond in propane.[17,19,20] The detailed reaction mechanism is a matter of ongoing discussion bearing models that consider specific metal positions on the basal plane of the M1 phase as active sites.[21–23] In different schemes, M1 is regarded as a reservoir of chemically and structurally dynamic active sites formed under reaction conditions on the entire M1 surface.[24–26]

In the present study, we are addressing the question of whether the framework and surface composition of phase-pure M1 MoVTeNb oxide are related to the yield of acrylic acid in selective oxidation of propane. For this purpose, catalysts have been prepared by hydrothermal synthesis altering the reaction conditions in a broad range including the application of high temperatures and pressures in superheated water vapor and exploring the phase width of the M1 structure. By keeping strict the phase purity, the effect of metal site occupancy in the M1 framework on surface composition and catalytic behavior was investigated, revealing that the metal stoichiometry at the surface responds dynamically and reversibly to the gas-phase composition. The relationship between chemical composition and catalytic performance of M1 is discussed on the basis of the concept of site isolation in the context of electronic structure and termination of M1.

Experimental Section

The catalysts have been prepared by hydrothermal synthesis as described previously.[9] Briefly, a suspension was prepared by mixing the aqueous solutions of the metal salts with a nominal Mo/V/Te/Nb molar ratio of 1/0.23−0.25/0.09−0.23/0.07−0.12. After hydrothermal synthesis at 423−448 K for 48 h, the resultant dark blue slurry was filtered, washed with bidistillated water, and dried at 353 K for 16 h. Starting from the as-derived solid, 3 g of the crystalline product was obtained by heat-treatment in inert gas with a flow of 100 mL min^{-1} for 2 h at 873 K or at 923 K (heating rate 15 K min^{-1}), either with or without previous calcination in synthetic air for 1 h at 548 or 598 K (heating rate 10 K min^{-1}). The thermal treatment was carried out in a rotating furnace (Xerion).

In modification of the classical hydrothermal synthesis, MoVTeNb mixed oxide was prepared by treatment of an oxidized precursor in superheated water vapor. The precursor was obtained by spray-drying a 0.54 M metal oxalate solution with a nominal Mo/V/Te/Nb molar ratio of 1/0.3/0.23/0.13 followed by calcination in flowing synthetic air (100 mL min^{-1}) for 1 h at 548 K (heating rate 5 K min^{-1}) in the rotating oven. The calcined solid was mixed with the appropriate amount of water and treated for 2 h at $p = 20$ MPa and 773 K (heating rate 5 K min^{-1}). The resulting material was thermally treated at 873 K (heating rate 15 K min^{-1}) in flowing Ar (flow rate 100 mL min^{-1}) for 2 h in the rotating furnace.

Furthermore, phase-pure M1 prepared by the patented spray-drying method[6,27] and purified according to ref 28 has been generated.

For selective oxidation of propane to acrylic acid, 0.5 g of the catalysts was pelletized (8 ton on a round surface 3 cm in diameter), crushed, sieved (200−400 μm), and loaded into a quartz fixed bed reactor with an inner diameter of 4 mm. The feed was composed of propane/oxygen/nitrogen/steam in a molar ratio of 2.8/6.4/50.8/40. At a reaction temperature of 673 K, the gas hourly space velocity (GHSV) was varied between 1200 and 5000 h^{-1}. The products were analyzed by gas chromatography. Inorganic gases and C_1−C_3 hydrocarbons have been analyzed with a thermal conductivity detector using a molecular sieve column and a Porapak Q column, respectively, for separation. Oxygenated products have been detected applying a HP-FFAP column and a flame ionization detector.

XRD was measured on a STOE STADI-P transmission diffractometer with a focusing primary Ge(111) monochromator applying Cu Kα1 radiation ($\lambda = 1.5406$ Å). Data analysis was performed using the software package Topas (v2.1, Bruker AXS).

A Hitachi S-5200 with a PGT Spirit EDX system and a Hitachi S-4800 with an EDAX Genesis EDX detector were used for scanning electron microscopy (SEM) studies. The samples were deposited on carbon tape. Images were acquired at 2 kV to optimize surface resolution, while energy dispersive X-ray spectroscopy (EDX) was carried out with an accelerating voltage of 10 kV. The compatibility of the two different EDX systems was confirmed by analyzing a standard MoVTeNb oxide catalyst. Furthermore, elemental analysis performed with ICP-OES (SCG Fresenius GmbH) for a number of catalysts gave consistent results.

Transmission electron microscopy was carried out on a Philips CM 200 FEG TEM operated at 200 kV. The microscope was equipped with a Gatan CCD camera for image acquisition and an EDAX Genesis EDX system. The specimens were prepared by dry dispersing the catalyst powder on a standard copper grid coated with holey carbon film. HRTEM image simulations were calculated using JEMS.

A depth profile of the elemental composition was recorded applying X-ray photoelectron spectroscopy (XPS). By varying the kinetic energy between 170 and 470 eV separately for each core level, escape depths (63% of detected signal comes from this depth) of ca. 0.8 nm (denominated as surface) and ca. 1.6 nm (denominated as subsurface) were probed. Valence band spectra have been also acquired using different excitation energies. The experiments have been performed in the presence of 20−30 Pa of oxygen or mixtures of $C_3H_8(C_3H_6)/O_2/H_2O$ at

TABLE 1: Metal Stoichiometry of Phase-Pure M1 Catalysts As Determined by EDX and ICP-OES

catalyst ID/reference	synthesis method	Mo [at. %]	V [at. %]	Te [at. %]	Nb [at. %]
939	hydrothermal	51 ± 4.3	15 ± 1.3	11 ± 2.8	23 ± 5.1
1761	hydrothermal	53 ± 1.9	12 ± 0.9	15 ± 2.6	20 ± 1.7
1434[a]	hydrothermal	54	16	10	20
1886	hydrothermal	58 ± 3.0	13 ± 1.1	12 ± 2.6	17 ± 1.6
1650	hydrothermal	58 ± 0.9	15 ± 0.5	10 ± 1.6	17 ± 1.4
6059	spray-drying	62 ± 1	17 ± 0.4	7 ± 0.1	14 ± 0.8
3030	SWVT[b]	63 ± 3.8	22 ± 5.1	6 ± 1	9 ± 0.9
5511	hydrothermal	66 ± 0.6	17 ± 0.2	7 ± 0.3	10 ± 0.3
6142	hydrothermal	77	23	0	0
ref 8	M1 unit cell composition	71	11	9	9
ref 8	M2 unit cell composition	55	18	23	4

[a] ICP-OES results. [b] Superheated water vapor treatment.

TABLE 2: Lattice Constants of Phase-Pure M1 Catalysts

catalyst ID/reference	synthesis method	*a* [Å]	*b* [Å]	*c* [Å]
939	hydrothermal	21.205(2)	26.680(3)	4.0051(3)
1761	hydrothermal	21.208(5)	26.741(6)	4.0016(6)
1434	hydrothermal	21.196(4)	26.698(5)	4.0099(5)
1886	hydrothermal	21.199(3)	26.710(4)	4.0131(4)
1650	hydrothermal	21.199(4)	26.708(5)	4.0102(6)
6059	spray-drying	21.1255(16)	26.615(2)	4.0137(2)
3030	SWVT[a]	21.121(2)	26.614(2)	4.0138(3)
5511	hydrothermal	21.1035(15)	26.5798(19)	4.0157(2)
ref 8	M1	21.134(2)	26.658(2)	4.0146(3)

[a] Superheated water vapor treatment.

the beamline U49-/2-PGM1 of BESSY II synchrotron (Berlin, Germany). Details of the setup have been published earlier.[29] The error bar of the absolute elemental composition can be estimated up to 25% due to uncertainties in the monochromatic photon flux, cross sections, and peak areas. However, only the uncertainty in the peak area determination contributes to relative uncertainties in an experimental series (different conditions with the same catalyst or different catalysts at the same conditions), and therefore the relative error bar in the XPS figures and in Table 3 can be estimated to be approximately 2%.

Specific surface areas of the catalysts were measured by nitrogen physisorption using an AUTOSORB-1-C physisorption/chemisorption analyzer (Quantachrome). Prior to nitrogen adsorption, the samples were degassed at 353 K for 2 h. Generally, 11 points have been considered in the linear range of the adsorption isotherm to calculate the surface area according to the BET method.

Results

Metal Stoichiometry of the M1 Framework. The quinternary MoVTeNb oxide catalysts studied in the present work are phase-pure M1 materials, characterized by high crystallinity.[9] The chemical composition of the catalysts measured by EDX or ICP-OES is summarized in Table 1. The materials are arranged top down with increasing Mo content. The variation in chemical composition is reflected in the lattice constants summarized in Table 2. Because of the complexity of the orthorhombic structure and the multiplicity of options for different metal site occupancies, systematic variations in the lattice constants are not expected. However, with increasing Mo content, the lattice constants *a* and *b* tend to decrease. No systematic variation is observed in the parameter *c* that reflects the stacking height along the [001] direction.

Tailoring the composition of M1 has been achieved by applying the three different preparation methods explained in the Experimental Section. Within the explored reaction parameter space, the flexibility of the M1 stoichiometry has been established to be restricted to a certain compositional area that is illustrated in the diagram in Figure 1. The molybdenum content varies between 51 and 77 at. %. In most of the M1 catalysts, the niobium concentration even exceeds 9 at. % with respect to the metals (Table 1), which represents the limit for complete occupation of pentagonal bipyramidal metal positions in the M1 unit cell.[8] Therefore, in the corresponding highly crystalline M1 catalysts, niobium partially occupies metal sites with octahedral oxygen coordination, which has been confirmed by EXAFS.[9] Tellurium is situated in the hexagonal and heptagonal channels of the M1 framework. Accordingly, the tellurium content of M1 can be changed independently from the other metals by approaching complete occupation of the potential positions. In the present study, the total Mo and Nb content has been kept constant at approximately 75 at. % with respect to the metals, while the content of Te and V was altered. The Te content was varied between 6 and 15 at. %. Attempts to increase the vanadium content above 25 at. % failed so far due to segregation of the $V_{0.95}Mo_{0.97}O_5$ phase when higher vanadium concentrations were applied in the synthesis. The chemical composition of phase-pure M1 catalysts near the surface has been studied by photoelectron spectroscopy. Because

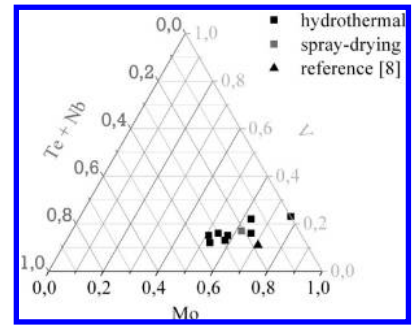

Figure 1. Metal stoichiometry (at. %) of M1 catalysts prepared by different methods. The Te- and Nb-free MoV oxide with orthorhombic structure was prepared for reference.

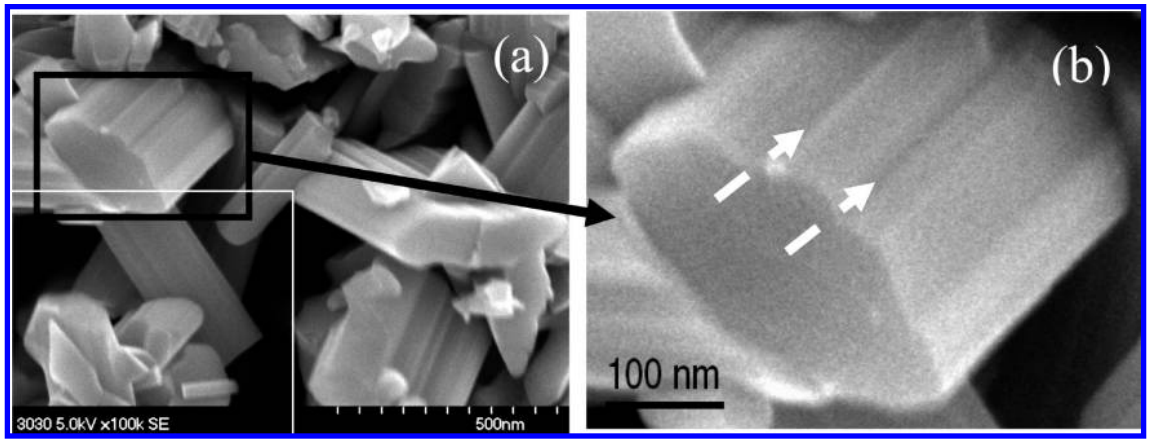

Figure 2. SEM images of phase-pure M1: (a) prismatic shape and (b) steps on the sides of the particles parallel to the [001] direction.

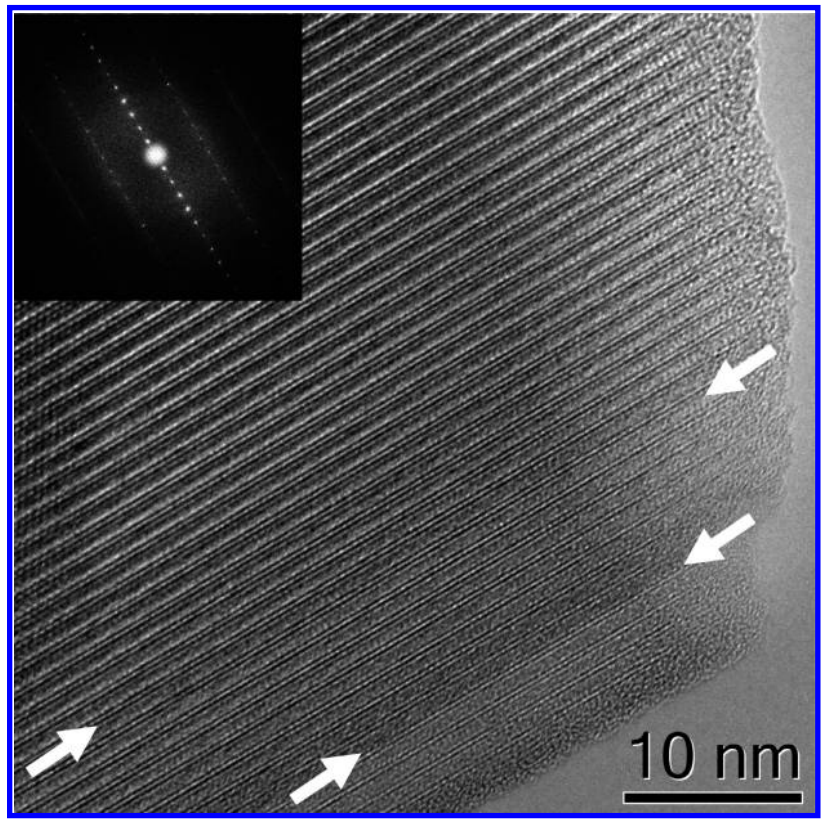

Figure 3. HRTEM image of the lateral surface of a prismatic M1 particle; zone axis ~[214]. The steps are indicated by arrows.

the measured surface composition is affected by microstructure and termination of M1, the microstructural characteristics of the M1 catalysts will be described in the following section prior to the XPS experiments.

Microstructure of Phase-Pure M1 Catalysts. Figure 2 shows representative SEM images of the primary M1 particles. The mixed oxide crystallizes predominantly in a prismatic morphology characterized by a high aspect ratio (length/diameter ratio) of the particles. The crystals are not always isolated entities. They form agglomerates and interlock in some cases. Because of the high aspect ratio of the material, the exposed surface area is comprised of mainly the lateral surface of the prisms terminated by {*hkl*} planes. Along the sides, steps of different dimensions parallel to the length axis in [001] direction are observed. The largest steps are tens of nanometers high, comprising several unit cells of M1 (arrows in Figure 2b). On the terraces, contrast variations are observed, which are assumed to be steps of subunit cell dimensions. High-resolution transmission electron microscopy (Figure 3) shows that these surface steps are indeed revealed as crystallographic steps propagating along the length axis of the prismatic structures. Such steps provide sites of distorted coordination generally assumed to be centers of catalytic activity.

As previously reported,[24] a characteristic termination has been observed by HRTEM on the entire surface of MoVTeNb mixed oxides. In particular, the particles are covered completely by a restructured surface layer as shown in Figure 4a. To verify that the formation of this layer is not an artifact caused by the electron beam, a M1 crystallite was continuously irradiated at ca. 5×10^{-14} A/nm^2 with electrons over an extended period of time (Figure 4a,b). The thickness of the surface layer was plotted as a function of the irradiation time (Figure 5). A constant increase in the thickness of the surface layer (~0.06 nm min^{-1}) was observed, indicating that the layer is in part an effect of the electron beam. However, extrapolating to $t = 0$, a finite thickness is estimated, revealing that there is an intrinsic

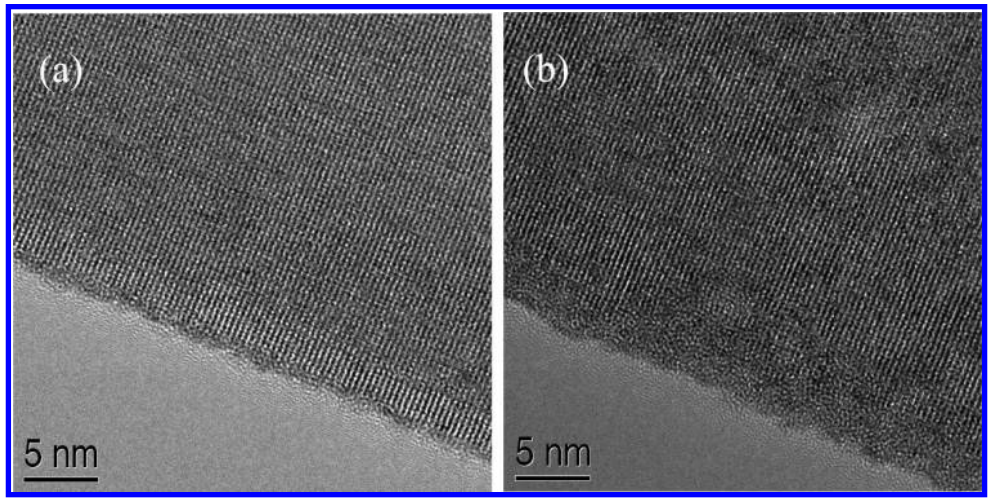

Figure 4. TEM images of M1 after (a) 1 min and (b) 31 min exposure time to the electron beam at a current density of ca. 5×10^{-14} A/nm^2.

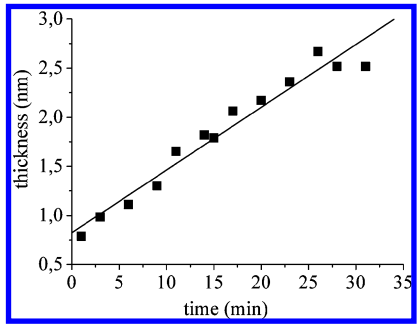

Figure 5. Thickness of the restructured termination of the M1 particles as a function of the exposure time to the electron beam at ca. 5×10^{-14} A/nm^2.

terminating structure different from that of the M1 crystal structure (Figure 5). The thickness of this surface layer is roughly 0.7 nm, which corresponds to the escape depth of surface-sensitive X-ray photoelectron spectroscopy (approximately 0.8 nm).

Metal Stoichiometry Near the Surface. The chemical composition of M1 (Table 1) affects the nature of the active sites on the surface and, therefore, the catalytic properties. Table 3 represents the surface composition of a number of M1 catalysts measured at 298 K by in situ photoelectron spectroscopy in the presence of 20 Pa oxygen, probing an escape depth of 0.8 nm that comprises nearly the restructured surface layer elucidated by HRTEM. In agreement with a surface structure different from M1, the surface stoichiometry is not in accordance with the M1 unit cell formulation (Table 1).[8] In line with vacuum XPS experiments,[12,14,28,30–32] the surface is enriched in tellurium and depleted in vanadium and niobium. In the presence of oxygen or oxygen-containing mixtures in the gas phase, beam damage has not been observed during the XPS measurements as verified by probing different spots on the catalyst surface. The concentration of tellurium on the surface correlates with the Te content in the bulk as shown in Figure 6. The same holds for the other metals. For clarity, Mo and Nb concentrations are not included in the plot.

Relations between Chemical Composition and Catalytic Properties. Table 4 summarizes the catalytic properties of the phase-pure M1 catalysts in the oxidation of propane to acrylic acid at 673 K in the presence of 40 vol. % steam in the feed. The majority of the catalysts show high activity in propane conversion. For the same contact time, the conversion tends to increase with increasing surface area of M1. However, a linear correlation between specific surface area and propane conversion is not evident, indicating that other factors such as variations in elemental composition contribute to the observed differences in activity. Despite phase purity and high crystallinity, the yield of acrylic acid obtained on the M1 catalysts varies between 7% and 44%.

In Figure 7, the yield of acrylic acid normalized to the specific surface area is plotted as a function of the percentage of Te (Figure 7a) and Mo (Figure 7b) in the crystalline M1 framework (open symbols) and at the surface (filled symbols). As a vague trend, the yield progressively increases with increasing Te content in the solid. The correlation is more evident when the percentage of Te at the surface is considered. In contrast, the yield of acrylic acid decreases with increasing percentage of Mo in the bulk and at the surface. It should be mentioned that no clear correlation is observed between the yield of acrylic acid and the fraction of the M1 constituents V and Nb, neither at the surface nor in the bulk.

In the mechanistic concept proposed by Grasselli et al.,[18] the cooperation of isolated vanadyl species and Te^{4+} sites has been regarded to be of great importance in the formation of the intermediate propylene by abstraction of hydrogen via a propyl radical. In Figure 8, the molar ratio of Te and V is plotted versus the yield of acrylic acid normalized to the specific surface area of the catalysts. As a weak tendency, the yield of acrylic acid increases with increasing Te/V molar ratio in the crystalline framework (open symbols). In contrast, a clear correlation is evident at the surface that reflects an increase in the yield of acrylic acid with increasing Te/V ratio (filled symbols), emphasizing the importance of diluted vanadia species for the selective formation of acrylic acid.

Surface Stoichiometry and Valence Band Spectra in the Presence of the Reactants. In situ XPS quantification probed in the presence of 25−30 Pa of the reactants at 623 K (Figure 9, section A) revealed that the chemical composition of the surface layer of the M1 crystals responds dynamically to the composition of the gas phase. A depth profile of M1 was analyzed by applying different excitation energies, corresponding to an escape depth of approximately 0.8 nm (denominated as surface, Figure 9a) or 1.6 nm (denominated as subsurface, Figure 9b). Moreover, the same M1 catalyst has been investigated after being tested in propane oxidation using a fixed bed reactor at 0.1 MPa (Figure 9, section B). The XPS spectra of the utilized M1 catalyst were recorded at 298 K in the presence of 30 Pa of oxygen.

TABLE 3: Surface Metal Stoichiometry of Phase-Pure M1 Catalysts As Determined by XPS (Escape Depth Approximately 0.8 nm) at 298 K and at $p_{O2} = 30$ Pa

catalyst ID	synthesis method	Mo [at. %]	V [at. %]	Te [at. %]	Nb [at. %]
939	hydrothermal	41	11	38	10
1761	hydrothermal	57	9	23	11
6059	spray-drying	65	12	13	10
3030	SWVT[a]	71	12	9	8

[a] Superheated water vapor treatment.

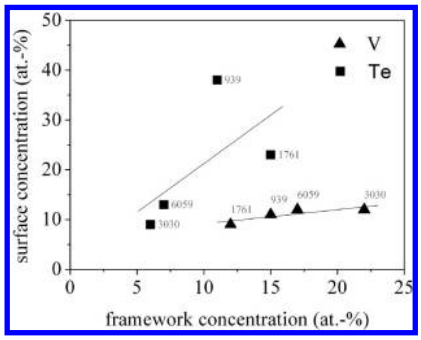

Figure 6. Near surface concentration of Te and V determined by XPS (escape depth 0.8 nm) at $T = 298$ K, $p = 30$ Pa O_2 as a function of the concentration in the crystalline M1 framework measured by EDX.

The surface of M1 in the presence of 30 Pa of O_2 before admission of propane is composed of approximately 60 at. % molybdenum (Table 3, Figure 9a). As compared to the crystalline bulk (Table 1), the tellurium content on the surface is significantly increased (approximately 20 at. %, Figure 9a). After admission of propane and heating to 623 K, the surface concentration of tellurium is further enhanced at the expense of molybdenum, which is even more noticeable in the presence of steam. As the steam is removed from the feed and propane is replaced by propylene keeping the temperature constant at 623 K, the tellurium fraction decreases in favor of molybdenum, close to the initial composition measured in O_2. The concentrations of vanadium and niobium remain relatively constant in the different reaction media. In contrast to what occurs on the surface, the tellurium content in the subsurface decreases after the addition of propane to the oxidative atmosphere in favor of molybdenum (Figure 9b). Apparently, the subsurface supplies tellurium to the surface and is, therefore, depleted in tellurium as compared to the surface, but the Te content is still enhanced in relation to the bulk. However, following the addition of steam, the tellurium content increases again at the expense of molybdenum as is the case at the surface. These observations may reflect the mobility of tellurium that seems to migrate throughout the hexagonal and heptagonal channels toward the surface, particularly in wet reaction atmosphere.

An elemental composition of the surface that deviates from the bulk composition is also confirmed by XPS analyses of the quenched catalyst, which was collected after the catalytic test in a fixed bed reactor at 0.1 MPa (Figure 9a, B). The surface composition of the used M1 is similar to the composition measured in the in situ experiment in the presence of steam. The subsurface composition of the used M1 catalyst is not very different from the surface composition due to equilibration under steady-state conditions (Figure 9b, B).

Table 5 shows the binding energies in comparison with reference binary oxide materials probed also in situ under oxygen at elevated temperature. In the presence of propane and oxygen in the gas phase at reaction temperature, the Mo 3d binding energy is shifted only by 0.4 eV relative to the position of MoO_3. On the basis of a second component at approximately 231.0 eV, the concentration of Mo^{5+} in M1 has been estimated to be below 5%. However, the chemical formula $Mo_{1.00}V_{0.26}Nb_{0.17}Te_{0.09}O_{4.0}$ determined by ICP-OES and carrier-gas hot-extraction (CGHE) suggests formal reduction of 25% Mo in the bulk when V and Te are assumed to be in the formal oxidation state 4+, and Nb in the formal oxidation state 5+. The binding energy of niobium is slightly lower than that of the corresponding binary Nb_2O_5 most likely related to final state effects being operative in defining the niobium binding energy. The binding energy of tellurium is slightly higher relative to TeO_2, possibly indicating an enhanced ionic character of the Te−O bond in M1. In accordance with studies on the bulk oxidation states of the elements in M1 by XANES[28] and ESR,[33] vanadium was mainly observed in the formal oxidation state 4+ on the surface of M1 also in the presence of the reactants.

Synchrotron radiation-based valence band spectra of M1 in the presence of propane, oxygen, and water vapor at 623 K are presented in Figure 10. The spectra were acquired at different excitation energies. For reference, the spectrum of MoO_3 at excitation energy of 700 eV (dotted line) was recorded in the presence of 30 Pa O_2 at elevated temperature. Gas-phase contributions are responsible for peaks above 10 eV, and for the peak at 7 eV in the 180 eV spectrum. The valence band structure of M1 changes with the excitation energy. With decreasing excitation energy, the intensity in the region of 6−10 eV decreases, while the signal in the region of 6−2 eV is enhanced. Analogue phenomena observed when measuring synchrotron radiation-based valence band spectra of MoO_3[26] have been attributed to attenuation of Mo 4d orbitals and amplification of O 2p orbitals, respectively. The effect has been explained by excitation energy-dependent variations in the cross section of the orbitals[26] and indicates a significant population of the Mo 4d orbitals. Moreover, the assignment of the Mo 4d and O 2p components in the experimental valence band structure of MoO_3 is in perfect agreement with DFT cluster calculations that model the MoO_3 (010) surface.[34] The spectrum of M1 at 180 eV excitation corresponds mainly to oxygen orbitals, whereas at high-energy excitation (710 eV) the spectrum has a considerable contribution of metal d orbitals (Figure 10). The overlap of 2p and 4d orbitals indicates enhanced electron density between the involved lattice atoms; that is, it reveals the partial covalent character of the bonding in the solid. M1 bears substantial resemblance with MoO_3 in the excitation energy dependency of the valence band spectra,[26] which points to a similar partial covalent character of the metal−oxygen bonds in MoVTeNb oxides. The appearance of intensity in the band gap at approximately 1 eV as an intrinsic feature of M1 even at room temperature is attributed to d orbital contributions of metal atoms in a formally reduced state. The corresponding region is magnified in the inset in Figure 10. The weak signal in the reference MoO_3 spectrum (dotted line) is indicative of oxygen vacancies on the MoO_3 surface.[34] The intensity is substantially enhanced in the spectra of M1 because for M1 the peak is dominated by formally reduced Mo and, in particular, V sites. The peak profile changes with the excitation energy, providing

TABLE 4: Catalytic Properties of M1 MoVTeNb Mixed Oxides in Selective Oxidation of Propane to Acrylic Acid at 673 K and a Feed Composition of Propane/Oxygen/Nitrogen/Steam = 2.8/6.4/50.8/40 mol %

catalyst ID	contact time [g_{cat}·s/mL]	X_{C3H8} [%]	S_{AA} [%]	Y_{AA} [%]	BET [m^2/g]	C_3H_8 consumption rate [mmol/g_{cat}·h]	acrylic acid space time yield [mmol/g_{cat}·h]	C_3H_8 consumption rate [mmol/g_{cat}·m^2]
1761	3	18	70	13	1.0	0.27	0.19	0.27
939	3	38	73	28	2.0	0.57	0.42	0.29
1650	3	56	79	44	2.5	0.84	0.66	0.34
1434	3	52	79	41	4.0	0.78	0.62	0.20
5511	3	52	58	30	5.9	0.84	0.49	0.14
1886	0.75	6	100	6	1.4	0.39	0.39	0.28
3030	0.75	49	73	36	6.7	2.94	2.15	0.44
6059	0.72	41	62	25	8.8	2.70	1.70	0.31

further evidence for differences in the distribution of reduced Mo and V centers in surface and subsurface.

Discussion

In nanocrystalline MoVTeNb oxide catalysts for selective oxidation of propane to acrylic acid, elaborate structural chemistry is combined with considerable chemical complexity.

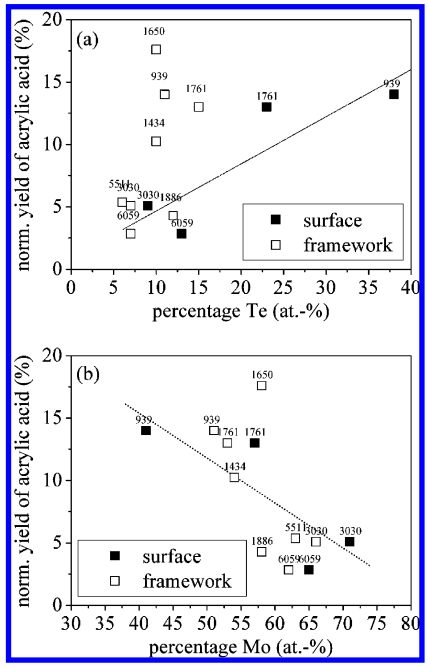

Figure 7. Yield of acrylic acid normalized to the specific surface area of the catalysts in the oxidation of propane at 673 K over phase-pure M1 as a function of (a) the Te percentage and (b) the Mo percentage in the crystalline M1 framework (open symbols) and at the surface (filled symbols, escape depth 0.8 nm).

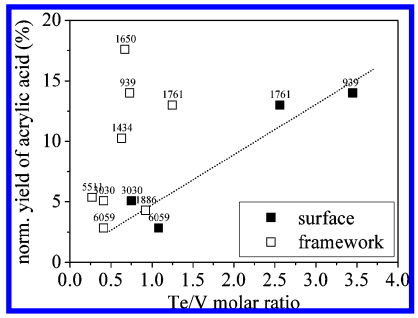

Figure 8. Yield of acrylic acid normalized to the specific surface area of the catalysts in the oxidation of propane at 673 K over phase-pure M1 as a function of the Te/V ratio in the crystalline M1 framework (open symbols) and at the surface (filled symbols, escape depth 0.8 nm).

In the present study, the chemical composition was varied, resulting in homogeneous, isostructural materials within the explored phase width of the M1 structure (Figure 1) with different metal site occupation for all four metal components. These differences are reflected in the variation of the lattice parameters (Table 2) and in the chemical composition at the surface (Table 3), showing a reasonable correlation between the concentrations of the metals in the crystalline bulk as analyzed by EDX and in the near surface region (escape depth 0.8 nm) as measured by surface-sensitive XPS (Figure 6). The slopes of these correlations are different from unity, which is indicative of a surface stoichiometry that is different from the bulk, and which is further deviating from the crystallographic stoichiometry of the M1 unit cell (Table 1). In particular, catalysts with

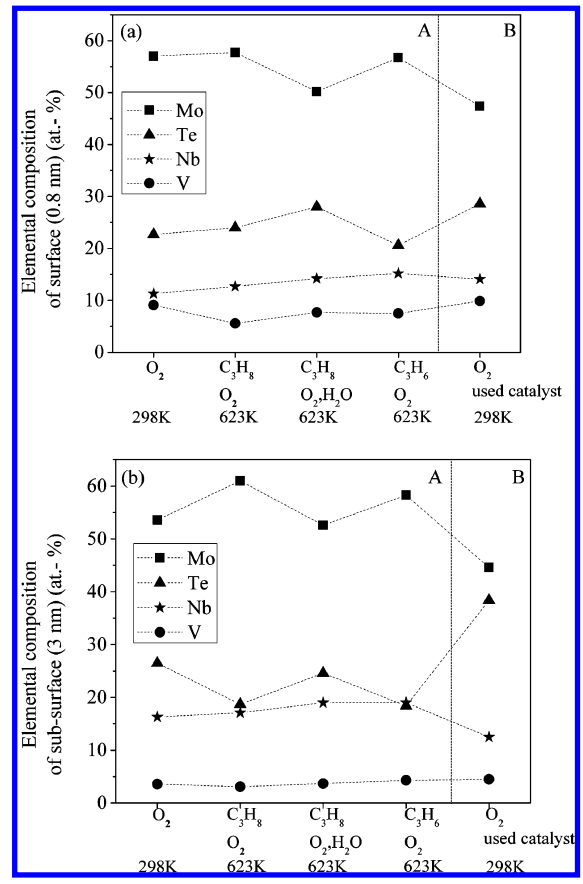

Figure 9. Quantification of the elemental composition of a M1 catalyst (ID 1761) by in situ XPS (at. %) (section A) at different layer depths: (a) surface (escape depth of ca. 0.8 nm) and (b) subsurface (escape depth of ca. 1.6 nm). The following reaction conditions were applied: measurement before admission of propane at 298 K and $p(O_2) = 30$ Pa; measurement at 623 K with molar ratio hydrocarbon:O_2 = 1:2, p = 20 Pa; $p(H_2O) = 10$ Pa; an oxygen pressure of 30 Pa was applied in the ex situ experiment (section B, used catalyst).

TABLE 5: Binding Energies of the Elements in M1 MoVTeNb Oxides Probed by XPS in the Presence of the Reactants at 298 K (ID 6059) and at 623 K (ID 1761 and 1886) Utilizing Low Kinetic Energy Electrons (Surface-Sensitive Mode, Escape Depth 0.8 nm)[a]

material (catalyst ID) /gas phase	O1s (eV)	V2p (3/2) (eV)	Mo3d (5/2) (eV)	Nb3d (5/2) (eV)	Te3d (5/2) (eV)
V_2O_5	530.1	517.2			
MoO_3	530.5		232.6		
Nb_2O_5	530.1[b]			207.2[b]	
TeO_2	530.1−530.4[c]				575.9[c]
M1 (ID 6059) O_2	530.4	516.3	232.6	206.6	576.3
M1 (ID 1761) $C_3H_8 + O_2$	530.1	516	232.3	206.4	576.1
M1 (ID 1761) $C_3H_8 + O_2 + H_2O$	530.1−530.2	516	232.2	206.4	576.2
M1 (ID 1886) $C_3H_8 + O_2 + H_2O$	530.2	516.1	232.3[d]	206.6	576.2

[a] The reference oxides were measured in the presence of O_2 at 623 K. [b] XPS Handbook: 530.6 eV; 207.5 eV. [c] XPS Handbook: 530.2 eV; 575.7 eV. [d] Measured in the absence of water vapor.

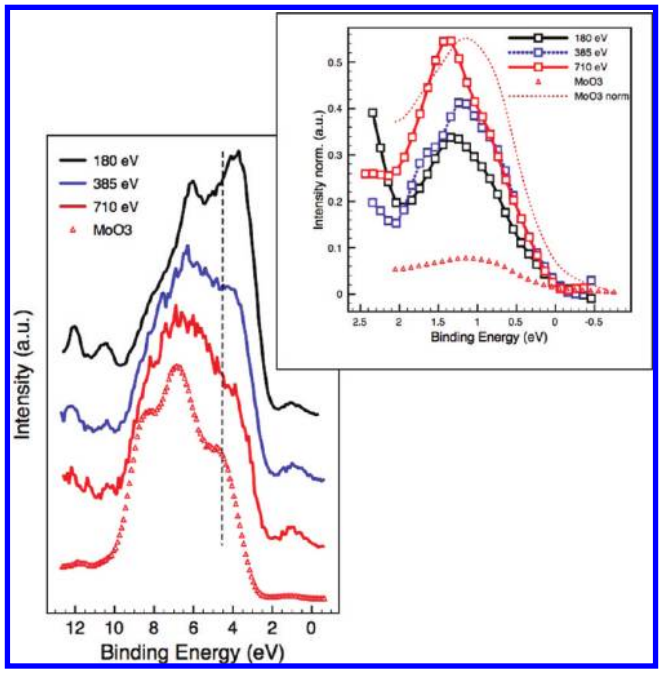

Figure 10. Excitation energy-dependent valence band spectra of M1 (catalyst ID 1761): (a) in the presence of propane, oxygen, and water vapor at 623 K; molar ratio propane:O_2 = 1:2, p = 20 Pa; $p(H_2O)$ = 10 Pa; (b) magnification of the energy range 2−0 eV; the spectrum of MoO_3 (dotted line) was acquired for reference at 700 eV in 30 Pa O_2 at 623 K; in the inset, the energy range from 0 to 2 eV is enlarged.

high Te content are substantially enriched in Te at the surface, illustrating an enhanced mobility of tellurium. The escape depth of the surface-sensitive XPS measurement of less than 1 nm probes the restructured surface layer of M1 revealed by HRTEM (Figures 4 and 5). The photoelectron spectroscopic experiments provide integral information with respect to the surface composition averaging possible differences in the chemical composition of the basal plane and the lateral surface of the catalyst particles. Low energy ion scattering (LEIS) measured in vacuum at room temperature in a previous study[25] revealed an even more enhanced enrichment of tellurium and vanadium in the topmost layer of the basal plane as compared to the entire M1 surface. Interestingly, the Te/V ratio on the basal plane and on the lateral surface was the same.[25] This requires mass transport on the surface of the activated catalyst as the M1 structure is characterized by structural anisotropy of the elemental distribution.

Increased percentage of Te and reduced fraction of Mo in the framework and, more pronounced, at the surface of M1 tend to result in higher yields of acrylic acid (Figure 7a and b). Moreover, a clear correlation between the Te/V molar ratio at the surface and the yield of acrylic acid has been found (Figure 8). Higher yields of acrylic acid have been achieved with increasing Te/V ratio; that is, the formation of acrylic acid is favored by progressive dilution of active vanadia sites on the surface. Apparently, tellurium-containing species either constitute the corresponding matrix that implements site isolation or are actively involved in the development of the catalytically relevant ensemble. On the basis of findings of in situ photoelectron spectroscopy (Figure 9), we propose that site isolation is realized through mobility of Te that is responsible for spatial isolation of vanadia sites on the surface of the crystalline M1 framework. We did not see any V segregation. Generally, vanadium is considered to be responsible for C−H activation. The binding energy of V in M1 at room temperature in the presence of oxygen is shifted by 0.9 eV to lower energies as compared to V_2O_5, and it decreases even further in the presence of propane and oxygen at reaction temperature (Table 5). The formation of the secondary propyl radical in the first step of propane oxidation has been attributed to V in the formal oxidation state 4+ on the M1 surface,[35] being fully consistent with spectroscopic observations and with studies of propane activation over model catalysts.[36,37]

Furthermore, the in situ XPS experiments revealed an enhanced mobility of Te especially in the presence of water vapor (Figure 9). Accordingly, the high selectivity to acrylic acid in the presence of steam in the feed may be caused by formation of mobile Te-containing clusters through hydrolysis of oligomeric $(TeO)_n$ species in the channels of the M1 structure, which migrate to the surface. Enhanced volatility of TeO_2 in water vapor has been attributed to the formation of gaseous $TeO(OH)_2$.[38] Thus, restructuring and possible formation of M−Te linkages and Te/V-containing clusters may provoke spatial isolation of vanadium-containing active sites embedded in an insulating matrix on the surface of the semiconductor M1. On the other hand, too high tellurium contents, such as in the Te-rich phase M2 (Table 1), might be detrimental due to site blockage by overgrowing all active sites. In a similar sense, a very recent study on the influence of tellurium on the catalytic behavior of Mo-containing tetragonal bronzes in the selective oxidation of propylene shows that the selectivity to acrolein increases when the Te/Mo ratio in the bulk increases up to ca. 0.03 and remains constant for catalysts with higher Te content.[39] A positive effect of Te additives on the selectivity to acrylic acid in propane oxidation has also been observed for other catalysts systems, such as V−P−O and Ni−Mo−O.[40]

The excitation energy-dependent valence band spectra of M1 MoVTeNb oxide (Figure 10) provide some insight into the electronic structure of this complex material and clearly reveal a substantial covalent character of the metal−oxygen bonds in M1. However, chemical and structural complexity of M1 and

the multitude of options for surface termination complicate the determination of surface states and molecular surface structure.

Conclusions

The sum of the present observations and the knowledge from literature may be combined to a unified picture about the material function of the M1 phase in propane oxidation:

(1) The M1 phase is a framework, stable in the chemical potential of the working catalyst and essential for sustained catalyst performance, but neither a dominant structure sensitivity (fraction of (001) faces in the catalyst)[25] nor a structure function correlation using the geometric surface area of the M1 phase as variable exists. This implies that the active sites are not an intrinsic component of the M1 structure but still require the existence of M1 for their operation.

(2) The acrylic acid yield is strongly positively correlated with the Te/V ratio and equally strongly anticorrelated with the Mo abundance, indicating that the active sites do not contain all constituent elements of the M1 phase.

(3) The chemical bonding in the structure is strongly covalent, meaning that no ionic differentiation between metal centers of the crystallographic structure exists. The strong covalence in the compound results in a high chemical and structural stability of the system that is absolutely critical with respect to the sometimes reducing and hydrothermal reaction environment that would tend to disintegrate and reduce the complex oxide. The covalence further allows the existence of defect states with respect to the hypothetical fully oxidized structure, resulting in a donor band of electrons exhibiting a small binding energy in the order of magnitude of their thermal excitation. These states classifying the solid as zero-bandgap semiconductor are required to activate molecular oxygen but need to be carefully controlled to guarantee kinetic control of the potentially detrimental activated oxygen against overoxidation.

(4) The strong covalence classifies the M1 system as a framework structure that contains at least some of the tellurium oxide units as true guest species in the sense that they can be removed without letting the structure collapse. The M1 system is thus a support for an active phase at its surface and a packaging structure for Te_xO_y species as critical components that are liberated from its "container" only and possibly reversible under reaction conditions. Embedded in this Te_xO_y surface species are vanadia species existing in geometric isolation. We assume polyoxo-metalate structures as models allowing several V atoms to be connected (V_xO_y species).

(5) From photoelectron spectroscopy and microscopic observations, we know that the zone of dynamics is limited to a thickness of about 1 nm. The remarkable stability of the active surface layer implies further that chemical bonds exist between the M1 bulk and the surface layer, which provide the gateway for the electron density from the electronic structure of the bulk M1 phase to the V_xO_y units.

These findings indicate that, despite the already high level of analytical description, the present work still lacks in analytical power as it would be necessary to know the electronic structure of the top surface under reaction conditions and it would be most relevant to observe the lateral elemental disposition with sub-nanometer resolution to identify the type of oxo-clusters constituting the surface. The still best surface probe is the reaction itself that has provided us with the insight that the active sites are not containing all chemical elements of the M1 phase.

The dynamic response of M1 to the chemical potential of the reaction creates an active surface and at special sites that are predetermined in the kinetics of the phase formation process also active sites. This scenario explains and respects all known facts about the M1 phase including the wide range of performances observed for structurally "identical" M1 phases and can be used to optimize the performance for which two independent lines of variables are predicted; the correct abundance of Te_xO_y is required, and the metal distribution in the M1 solid needs to allow the formation of a terminating surface at sites where vanadia dimers or similar clusters can form.

Both lines of variables are controlled by solid-state properties and likewise by the chemical potential of the operation. This explains the difficulty in conventional optimization strategies trying to optimize either via variation of chemical composition or by searching fixed optimized operation conditions. Both approaches neglect the interconnection between the variables and thus will not deliver the optimum performance. Only the combined control of synthesis kinetics with for every system individually optimized reaction conditions can exploit the optimum performance. This performance is still limited by the overall gradients in chemical potential found in plug flow reactor arrangements.

Acknowledgment. We thank Dr. Ayyamperumal Sakthivel, Till Wolfram, Dr. Yury V. Kolen'ko, and Dr. Zirong Tang for their help in catalyst preparation, and Gisela Lorenz and Daniel Brennecke for performing the nitrogen physisorption. Dr. Tulio Rocha is acknowledged for assistance in measurements of the photoelectron spectra. We thank Dr. Gudrun Auffermann, Max Planck Institute of Chemical Physics of Solids, Dresden, for chemical analysis.

References and Notes

(1) Novakova, E. K.; Védrine, V. C. In *Metal Oxides, Chemistry and Applications*; Fierro, J. L. G., Ed.; CRC Press: New York, 2006; p 414.

(2) Centi, G.; Cavani, F.; Trifirò, F. *Selective Oxidation by Heterogeneous Catalysis*; Kluwer Academic/Plenum Publishers: New York, 2001; p 363.

(3) Lin, M. M. *Appl. Catal., A* **2001**, *207*, 1.

(4) Tanimoto, M.; Himeji-shi, H.; Mihara, I.; Aboshi-ku, H.; Kawajiri, T.; Himeji-shi, H. EP 0711745 B1, 1996, to Nippon Shokubai.

(5) Tenten, A.; Hibst, H.; Martin, F.-G.; Marosi, L.; Kohl, V. DE 4405514 A1, 1995, to BASF.

(6) Ushikubo, T.; Nakamura, H.; Koyasu, Y.; Wajiki, S. U.S. Patent 5380933, 1995, to Mitsubishi Kasei Corp.

(7) Ushikubo, T.; Oshima, K.; Kayou, A.; Hatano, M. *Stud. Surf. Sci. Catal.* **1997**, *112*, 473.

(8) DeSanto, P.; Buttrey, D. J.; Grasselli, R. K.; Lugmair, C. G.; Volpe, A. F.; Toby, B. H.; Vogt, T. *Z. Kristallogr.* **2004**, *219*, 152.

(9) Celaya Sanfiz, A.; Hansen, T. W.; Rödel, E.; Timpe, O.; Trunschke, A.; Schlögl, R. *Top. Catal.* **2008**, *50*, 19.

(10) Murayama, H.; Vitry, D.; Ueda, W.; Fuchs, G.; Anne, M.; Dubois, J. L. *Appl. Catal., A* **2007**, *318*, 137.

(11) Loub, J. *Collect. Czech. Chem. Commun.* **1993**, *58*, 1717.

(12) Baca, M.; Pigamo, A.; Dubois, J. L.; Millet, J. M. M. *Top. Catal.* **2003**, *23*, 39.

(13) Oliver, J. M.; López-Nieto, J. M.; Botella, P. *Catal. Today* **2004**, *96*, 241.

(14) Ueda, W.; Vitry, D.; Katou, T. *Catal. Today* **2004**, *96*, 235.

(15) Ivars, F.; Solsona, B.; Rodríguez-Castellón, E.; López Nieto, J. M. *J. Catal.* **2009**, *262*, 43.

(16) Katou, T.; Vitry, D.; Ueda, W. *Catal. Today* **2004**, *91*−*92*, 237.

(17) Ueda, W.; Vitry, D.; Katou, T. *Catal. Today* **2005**, *99*, 49.

(18) Grasselli, R. K. *Catal. Today* **2005**, *99*, 23.

(19) Balcells, E.; Borgmeier, F.; Grisstede, I.; Lintz, H. G.; Rosowski, F. *Appl. Catal., A* **2004**, *266*, 221.

(20) Novakova, E. K.; Vedrine, J. C.; Derouane, E. G. *J. Catal.* **2002**, *211*, 234.

(21) Oshihara, K.; Hisano, T.; Ueda, W. *Top. Catal.* **2001**, *15*, 153.

(22) Guliants, V. V.; Bhandari, R.; Soman, R. S.; Guerrero-Pérez, O.; Bañares, M. A. *Appl. Catal., A* **2004**, *274*, 123.

(23) Grasselli, R. K.; Buttrey, D. J.; DeSanto, P., Jr.; Burrington, J. D.; Lugmair, C. G.; Volpe, A. F., Jr.; Weingand, T. *Catal. Today* **2004**, *91*−*92*, 251.

(24) Wagner, J. B.; Timpe, O.; Hamid, F. A.; Trunschke, A.; Wild, U.; Su, D. S.; Widi, R. K.; Hamid, S. B. A.; Schlögl, R. *Top. Catal.* **2006**, *38*, 51.

(25) Celaya Sanfiz, A.; Girgsdies, F.; Hansen, T. W.; Trunschke, A.; Schlögl, R.; Knoester, A.; Brongersma, H. H.; Looi, M. H.; Hamid, S. B. A. *J. Catal.* **2008**, *258*, 35.

(26) Teschner, D.; Vass, E. M.; Schlögl, R. In *Metal Oxide Catalysis*; Jackson, S. D., Hargreaves, J. S. J., Eds.; Wiley−VCH: Weinheim, 2009; p 487.

(27) Beato, P.; Blume, A.; Girgsdies, F.; Jentoft, R. E.; Schlögl, R.; Timpe, O.; Trunschke, A.; Weinberg, G.; Basher, Q.; Hamid, F. A.; Hamid, S. B. A.; Omar, E.; Mohd Salim, L. *Appl. Catal., A* **2006**, *307*, 137.

(28) Baca, M.; Millet, J. M. M. *Appl. Catal., A* **2005**, *279*, 67.

(29) Bluhm, H.; Hävecker, M.; Knop-Gericke, A.; Kleimenov, E.; Schlögl, R.; Teschner, D.; Bukhtiyarov, V. I.; Ogletree, D. F.; Salmeron, M. *J. Phys. Chem. B* **2004**, *108*, 14340.

(30) Millet, J. M. M.; Roussel, H.; Pigamo, A.; Dubois, J. L. *Appl. Catal., A* **2002**, *232*, 77.

(31) Botella, P.; Concepción, P.; López, J. M.; Moreno, Y. *Catal. Today* **2005**, *99*, 51.

(32) Ivars, F.; Botella, P.; Dejoz, A.; López Nietoa, J. M.; Concepción, P.; Vázquez, M. I. *Top. Catal.* **2006**, *38*, 59.

(33) Brückner, A. *Top. Catal.* **2006**, *38*, 133.

(34) Tokarz-Sobieraj, R.; Hermann, K.; Witko, M.; Blume, A.; Mestl, G.; Schlögl, R. *Surf. Sci.* **2001**, *489*, 107.

(35) Millet, J. M. M. *Top. Catal.* **2006**, *38*, 83.

(36) Magg, N.; Immaraporn, B.; Giorgi, J. B.; Schroeder, T.; Bäumer, M.; Döbler, J.; Wu, Z.; Kondratenko, E.; Cherian, M.; Baerns, M.; Stair, P. C.; Sauer, J.; Freund, H.-J. *J. Catal.* **2004**, *226*, 88.

(37) Argyle, M. D.; Chen, K.; Resini, C.; Krebs, C.; Bell, A. T.; Iglesia, E. *J. Phys. Chem. B* **2004**, *108*, 2345.

(38) Glemser, O.; Haeseler, R. v.; Müller, A. *Z. Anorg. Allg. Chem.* **1964**, *329*, 5.

(39) Botella, P.; García-González, E.; Solsona, B.; Rodríguez-Castellón, E.; González-Calbet, J. M.; López Nieto, J. M. *J. Catal.* **2009**, *265*, 43.

(40) Kaddouri, A.; Mazzocchia, C.; Tempesti, E. *Appl. Catal., A* **1999**, *180*, 271.

JP909352U